Neuron
Article

Use-Dependent Inhibition of Synaptic Transmission by the Secretion of Intravesicularly Accumulated Antipsychotic Drugs

Carsten H. Tischbirek,[1,6] Eva M. Wenzel,[1,6,7,8] Fang Zheng,[2,6] Tobias Huth,[2] Davide Amato,[1] Stefan Trapp,[4] Annette Denker,[5] Oliver Welzel,[1] Katharina Lueke,[1] Alexei Svetlitchny,[1] Manfred Rauh,[3] Janina Deusser,[2] Annemarie Schwab,[2] Silvio O. Rizzoli,[5] Andreas W. Henkel,[1,9] Christian P. Müller,[1] Christian Alzheimer,[2] Johannes Kornhuber,[1,6] and Teja W. Groemer[1,6,*]

[1]Department of Psychiatry and Psychotherapy
[2]Institute of Physiology and Pathophysiology
[3]Children's and Adolescents' Hospital
Friedrich-Alexander University of Erlangen-Nürnberg, 91054 Erlangen, Germany
[4]Department of Environmental Engineering, Technical University of Denmark, 2800 Kongens Lyngby, Denmark
[5]STED Microscopy of Synaptic Function, European Neuroscience Institute, 37077 Göttingen, Germany
[6]These authors contributed equally to this work
[7]Present address: Department of Biochemistry, Institute for Cancer Research, The Norwegian Radium Hospital, Oslo University Hospital, Montebello, 0310 Oslo, Norway
[8]Present address: Centre for Cancer Biomedicine, Faculty of Medicine, University of Oslo, Montebello, 0310 Oslo, Norway
[9]Present address: Department of Physiology, Faculty of Medicine, Kuwait University, Safat 13110, Kuwait
*Correspondence: teja.groemer@uk-erlangen.de
DOI 10.1016/j.neuron.2012.04.019

SUMMARY

Antipsychotic drugs are effective for the treatment of schizophrenia. However, the functional consequences and subcellular sites of their accumulation in nervous tissue have remained elusive. Here, we investigated the role of the weak-base antipsychotics haloperidol, chlorpromazine, clozapine, and risperidone in synaptic vesicle recycling. Using multiple live-cell microscopic approaches and electron microscopy of rat hippocampal neurons as well as in vivo microdialysis experiments in chronically treated rats, we demonstrate the accumulation of the antipsychotic drugs in synaptic vesicles and their release upon neuronal activity, leading to a significant increase in extracellular drug concentrations. The secreted drugs exerted an autoinhibitory effect on vesicular exocytosis, which was promoted by the inhibition of voltage-gated sodium channels and depended on the stimulation intensity. Taken together, these results indicate that accumulated antipsychotic drugs recycle with synaptic vesicles and have a use-dependent, autoinhibitory effect on synaptic transmission.

INTRODUCTION

Schizophrenia is a common, chronic, and severe mental disorder in which the brain loses its ability to discern the relevancy and origin of information, leading to misinterpretations, hallucinations, and delusions (Freedman, 2003; Kapur, 2003). It is believed that schizophrenia is caused by defects in various neurotransmitter systems (Lisman et al., 2008) and the combined action of multiple genetic defects and environmental factors (Harrison and Weinberger, 2005).

Typical antipsychotic drugs (APDs) such as haloperidol (HAL) and atypical APDs such as risperidone (RSP) and clozapine (CLO) are effective for treating the symptoms of schizophrenia. These drugs share a common action at dopamine (DA) receptors and also affect other neurotransmitter receptors (Lisman et al., 2008; Strange, 2001). During treatment, APDs accumulate in all brain regions (Gemperle et al., 2003; Kornhuber et al., 1999, 2006; Korpi et al., 1984; Tsuneizumi et al., 1992), and it has been hypothesized that the slow development of their full effect coincides with their tissue accumulation. The accumulation of weak-base psychotropic drugs in acidic organelles results from acidic trapping after intraluminal protonation of these weak bases with pKa values near to neutrality (de Duve et al., 1974; Schmalzing, 1988; Trapp et al., 2008). In addition, membrane potential differences could also drive the accumulation of cationic molecules in electronegative compartments (Duvvuri et al., 2004). Our current knowledge regarding the role of psychotropic drugs in synaptic vesicle recycling is limited, and the functional consequences of a hypothesized APD accumulation in synaptic vesicles (Rayport and Sulzer, 1995) have remained elusive. In the present study, we clarified the intravesicular accumulation of APDs and its effects on synaptic transmission. We show that the exocytic release of APDs from synaptic vesicles increased extracellular concentrations in freely moving rats and allowed them to inhibit synaptic transmission in a use-dependent manner. This paper describes the release and autoinhibitory action of APDs that accumulated in synaptic vesicles.

Table 1. Predicted Physicochemical Properties and Accumulation Factors of the APDs Used and the Model Substance LTR

Substance	Log K_{ow} Neutral	Log K_{ow} Ion	pK_a	Fold Accumulation in the Cytosol	Fold Accumulation in SV	Mean Therapeutic Plasma Concentration (μM)	Intravesicular Concentration (μM)
CPZ	5.2	2.1	9.41	19.7	123	0.55	67.7
RSP	2.9	0.2	7.89, 3.23	2.4	67.6	0.1	6.8
HAL	3.0	−0.1	8.25	2.7	84.4	0.03	2.5
CLO	3.5	2.0, −0.6	7.14, 5.34	2.75	74.1	1.28	94.9
LTR	2.1	−1.4	7.5	1.5	55.5	n.a.	2.8

APDs of different classes are weak bases and accumulate in synaptic vesicles as calculated using a cell model adapted from Trapp et al. (2008). When present in therapeutic plasma concentrations in the extracellular space, the drugs accumulate to intravesicular concentrations in the low micromolar range. K_{ow}, octanol water partition coefficient; pK_a, acid dissociation constant; SV, synaptic vesicle; n.a., not applicable.

RESULTS

Accumulation of APDs in Synaptic Vesicles

The subcellular distribution and accumulation of nonfluorescent APDs can be studied using fluorescent model substances with similar physicochemical properties (Rayport and Sulzer, 1995; Kornhuber et al., 2010), such as LysoTracker Red (LTR). When assessed by a Fick-Nernst-Planck equation-based model (Trapp et al., 2008), in which the parameters (such as the cytosolic and organelle diameters and the membrane potential) were adjusted to fit hippocampal synapses and vesicles, the accumulation of LTR was found to be similar to that of the four APDs: chlorpromazine (CPZ), HAL, RSP, and CLO (Table 1). When parting from therapeutic plasma concentrations, all of the APDs (Baumann et al., 2004) as well as LTR reached micromolar intravesicular concentrations. Incubating hippocampal neuronal cultures with 50 nM LTR resulted in a punctate fluorescence staining. Costaining with pH-dependent αSyt1-cypHer5 antibodies (Adie et al., 2002; Welzel et al., 2011), specific for the acidic lumen of synaptic vesicles (see Figures S1A–S1D available online), revealed correlated intravesicular fluorescence in synaptic boutons (Figure S1D) and brighter uncolocalized staining of other acidic compartments such as lysosomes (Figure 1A; colocalization analysis in Figures S1E and S1F). Ultrastructural analysis of cultures stained with photoconverted LTR confirmed accumulation in extrasynaptic organelles and synaptic vesicles with FM dye photoconversion-like staining (Figures 1B and S1B). Because of this low intrasynaptic volume fraction of synaptic vesicles, synaptic boutons were stained less prominently when compared with other acidic organelles. The LTR fluorescence at synaptic loci corresponded to a concentration of 180 nM LTR in solution (Figure S2), which is an underestimate because a synapse's volume comprises only part of the total focal volume. According to our model calculations, the addition of 50 nM LTR should result in an intravesicular concentration of ~2.8 μM, which agrees fairly well with the experimentally determined vesicular concentrations of 2.2 μM (Figure S2B).

To probe the accumulation of APDs more directly, we next tested the ability of APDs to displace the model substance from synapses. This experimental approach has been used to measure drug accumulation in lysosomes by Kornhuber et al. (2010) and in acidic organelles by Rayport and Sulzer (1995). As before, hippocampal neurons were incubated with 50 nM LTR and stained with αSyt1-cypHer5 (Figure 1C). The fluorescence of LTR-stained organelles decreased after the APD application (Figure 1E). Quantification of LTR fluorescence at synaptic sites after APD application revealed a dose-dependent fluorescence decrease (Figure 1D) that, in its amplitude, fitted the displacement of LTR from synaptic vesicles. The decrease was not explained by quenching of the dye by the APDs (Figure 1F) and was not observed at synapses labeled with the spectrally similar FM4-64 (Figures 1D and 1F).

Accumulation of APDs in Synaptic Vesicles Requires an Acidic Intravesicular Environment

The accumulation of APDs is thought to depend mainly on the low pH, but it could also be affected by electrical gradients. In addition to LTR treatment, synapses were labeled with both αSyt1-Oy488 (to quantify number of synaptic vesicles) and αSyt1-cypHer5 as a control for vesicular pH (Figure 2A). Quantification of the cypHer5 fluorescence signal demonstrated the efficient inhibition of vesicular acidification by 80 nM folimycin (Groemer and Klingauf, 2007; Sankaranarayanan and Ryan, 2001). Similarly, LTR fluorescence was significantly reduced at an increased intravesicular pH (Figures 2B and 2C). In contrast, depolarization by increased extracellular K^+ concentrations (~40mV) had no significant effect on synaptic LTR accumulation. Results from fluorescence imaging were mirrored by those obtained by model calculations (Figure 2D). Given that the synaptic vesicle volume comprises only 5.4% of the synaptic volume and that LTR also accumulates in the cytosol (Table 1), the LTR signal is predicted to be reduced to 55% over the entire synapse. This matches the experimentally obtained LTR fluorescence of 64.2% in the presence of folimycin reasonably well. We conclude that the accumulation of APDs is a result of the low intravesicular pH.

APD-Induced Displacement of LTR Is Not Due to the Dissipation of Vesicular pH Gradients

The dissipation of vesicular pH gradients by APDs themselves could contribute to the observed loss of LTR signal upon APD application. To test this possibility, we performed experiments with synaptopHluorin (spH), an optical probe consisting of a pH-sensitive GFP coupled to the intravesicular domain of synaptobrevin 2 (Miesenböck et al., 1998). First, we measured the spH fluorescence increase following full deacidification of the recycling pool to the external pH of 7.4 with folimycin. The spH fluorescence increased by 48.6% ± 10.2% (data from Welzel

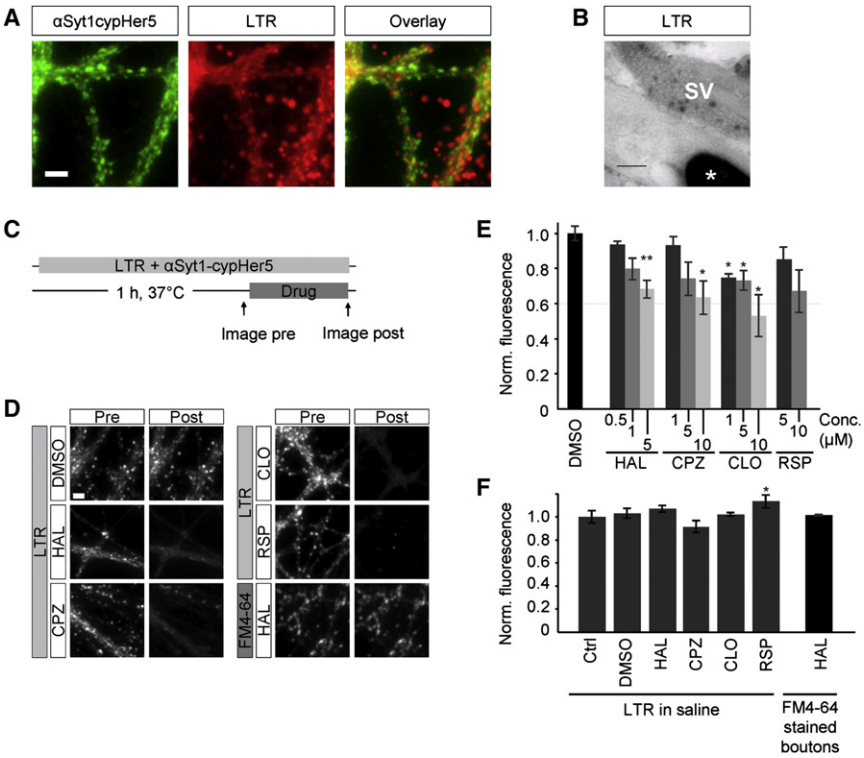

Figure 1. APDs Accumulate in Synaptic Vesicles

(A) Representative images of living hippocampal neurons. Left panel shows functional synapses that are fluorescently labeled with anti-synaptotagmin1-cypHer5 (αSyt1-cypHer5). Middle panel illustrates staining of the same region with 50 nM LTR. Right panel presents overlay of αSyt1-cypHer5 and LTR staining. LTR exhibits synaptic and extrasynaptic fluorescence.

(B) Photoconversion electron microscopy image of a hippocampal bouton labeled with LTR. Synaptic vesicles (SV) and large extrasynaptic vesicle-like structures (asterisk) are visible. Scale bar, 200 nm.

(C) Experimental procedure for (D) and (E). LTR fluorescence intensity was determined before and after the administration of APDs ("Drug") to viable LTR- and αSyt1-cypHer5-stained hippocampal neurons.

(D) Representative images of hippocampal neurons stained with 50 nM LTR or FM4-64 before (Pre) and after (Post) the administration of the drug or a vehicle (DMSO).

(E) Quantification of normalized mean synaptic LTR fluorescence intensity (n = 3 experiments each).

(F) Quantification of normalized (Norm.) fluorescence intensity of 1 μM LTR in saline and of FM4-64-stained synapses after the addition of the indicated substances (n = 3 experiments each). The tested APDs did not quench but instead displaced LTR from the synaptic terminals. Ctrl, control.

Error bars represent SEM. *$p < 0.05$, **$p < 0.01$, t tests. Scale bars in (A) and (D), 5 μm.

Please see Figure S1.

et al., 2011) in our imaging setup. This dissipation of the vesicular pH gradients was in accordance with the previously mentioned reduction of LTR fluorescence by folimycin (Figures 2B and 2C).

Accordingly, if the LTR fluorescence loss of, e.g., ~30% upon application of HAL 5 μM (Figure 2) was from the dissipation of vesicular pH gradients, then applying the drug would need to increase the intravesicular spH fluorescence comparably to folimycin. However, upon APD application only marginal differences in the spH fluorescence were observable, which were at the detection limit of our camera system (Figures 2E, 2F, and S3). The spH fluorescence, however, was very sensitive to small NH_4Cl-induced changes of the intravesicular pH (Figure 2E). Thus, the dissipation of the vesicular pH gradient by APDs in the concentrations used here is not a major factor contributing to the loss of LTR fluorescence.

APDs Are Released from Synaptic Vesicles via Exocytosis

Next, we tested whether accumulated weak bases can be released from synaptic vesicles via exocytosis. Hippocampal neurons stained with LTR and αSyt1-cypHer5 were electrically stimulated with varying intensities (600 action potential-like pulses [APs] at 30 Hz, 200 APs at 10 Hz, no Ca^{2+}; Figure 3A). We found that, as suggested previously by Schmalzing (1988), electrical stimulation led to a decrease in the LTR fluorescence at the synaptic sites, which depended on the presence of Ca^{2+} and increased with the strength of the stimulus (Figure 3B). The Ca^{2+} dependence, together with the fact that moderately depolarizing the cells with increased extracellular K^+ concentration did not significantly affect the accumulation of LTR in synaptic vesicles (Figure 1), argues against a passive LTR release resulting from the disruption of the electrical gradient across the synaptic membrane. Moreover, the different amounts of dye that were lost in response to varying stimulation intensities fit the expectations of vesicular exocytosis (Figure 3C). Importantly, intense LTR signals that did not colocalize with the synapse marker synaptotagmin1 and might stain lysosomes or other acidic cellular organelles did not show a decrease in fluorescence upon electrical stimulation (Figure 3D), again arguing for the release of LTR from synaptic vesicles via Ca^{2+}-dependent exocytosis.

Activity-Dependent HAL and Transmitter Release in Freely Moving Animals

To assess APD release after chronic treatment in vivo, we performed microdialysis in freely moving rats, which was followed by quantification of neurotransmitter and HAL. Animals were implanted with osmotic minipumps, which delivered HAL (0.5 mg/kg/d) for 14 days (Samaha et al., 2007), a dose that was shown to provide a brain DA D2 receptor occupancy similar to that required for human antipsychotic treatment action (Kapur et al., 2003). On day 14, triple-probe microdialysis was performed, measuring extracellular levels of HAL in the prefrontal

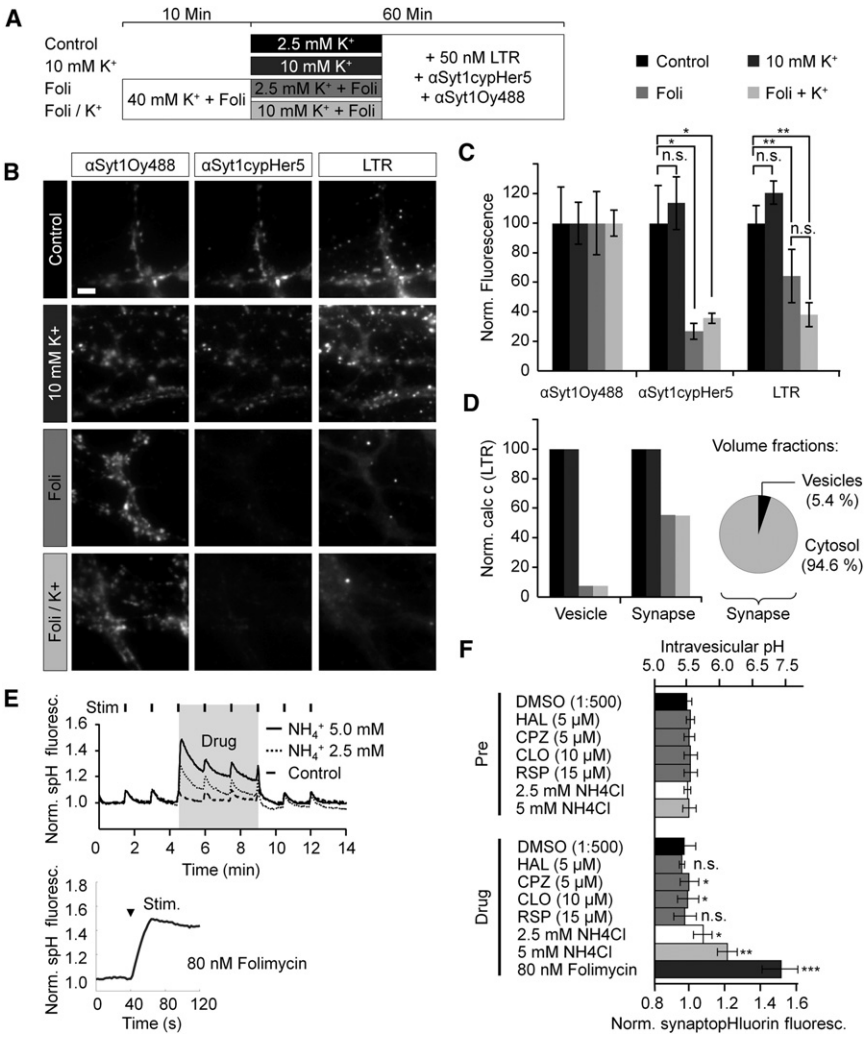

Figure 2. Acidic Intravesicular pH Is Needed for the Accumulation of APDs and Not Changed by APD Treatment

(A) Experimental procedure. Rat hippocampal neurons were stained with LTR in the presence or absence of the vATPase inhibitor folimycin (Foli, 80 nM) with physiological (2.5 mM) or elevated (10 mM) K^+ levels. To simultaneously visualize synapses and their acidification, the neurons were coincubated with anti-Syt1-Oy488 (Oyster 488) and an antibody with pH-dependent dye αSyt1-cypHer5.

(B) Representative images of hippocampal neurons stained as indicated in (A). Scale bar, 5 µm.

(C) Quantification of normalized (Norm.) mean synaptic fluorescence intensity in the four different staining paradigms (n = 3). Error bars represent SEM.

(D) Normalized calculated LTR concentrations in synaptic vesicles and whole synapses for folimycin and K^+ administration. The vesicle diameter, number of vesicles, and synapse volume used to calculate volume fractions were taken from Schikorski and Stevens (1997).

(E) Upper panel shows average spH fluorescence intensity profiles for the administration of ammonium chloride (NH_4Cl) (2.5 mM, n = 4, and 5.0 mM, n = 5) and control (n = 4). Constant perfusion with standard saline was switched to the vehicle or the NH_4Cl containing saline during minutes 4.5 and 9.0. Stim., electrical stimulation (50 AP, 10 Hz). Lower panel presents average spH fluorescence intensity profile. Cells were incubated with 80 nM folimycin to dissipate the intravesicular pH gradient of recycling vesicles. Stim., electrical stimulation (1,200 AP).

(F) pH changes by administration of the different APDs are limited to <0.1 pH. Baseline fluorescence levels and corresponding intravesicular pH before (Pre) and during (Drug) administration of substances. Indicated are DMSO (1:500), 5 µM HAL, 5 µM CPZ, 10 µM CLO, 15 µM RSP, 2.5 mM and 5.0 mM NH_4Cl (corresponding to a 0.4 and 0.7 pH change, respectively) and 80 nM folimycin (complete deacidification of the recycling pool of vesicles to a pH of 7.5).

Error bars represent the SD. *p < 0.05, **p < 0.01, ***p < 0.001, n.s. not significant, t tests.

Please see Figures S2 and S3.

cortex (PFC) and the dorsal striatum (DStr) and extracellular levels of DA and serotonin (5-HT) in the nucleus accumbens (NAc), as a reference for transmitter release (Figure 3E) (Amato et al., 2011). Baseline levels of HAL were 143.9 + 28.4 pg/ml in the PFC and 179.1 + 40.5 pg/ml in the DStr (n = 5), which was not corrected for recovery (in vitro, 84.7%). A 100 mM K^+ challenge, applied locally by reverse dialysis (Chen and Kandasamy, 1996), significantly increased the extracellular HAL concentrations compared to the baseline in the PFC (40 min samples, samples S3 and S4 versus baseline; $p < 0.05$) and DStr (40 min samples, samples S3 and S4, versus baseline; $p < 0.05$) during the K^+ challenge (Figure 3F). This was paralleled by an increase in extracellular DA (20 min samples, samples S5–S8, versus baseline; $p < 0.05$) and 5-HT levels (20 min samples, samples S5 and S6, versus baseline; $p < 0.05$) (Figure 3G). These data suggest that the extracellular HAL concentration in the brain is activity dependent after chronic HAL treatment in freely moving animals. It behaves similarly to the neurotransmitters DA and 5-HT. The different amounts of secreted HAL might reflect varying accumulation, release, or even receptor distribution properties, depending on the brain region. The activity-dependent increase of HAL concentrations in the dialysate from the synaptic cleft supports the idea of transient high APD concentrations, especially in close proximity to the vesicle fusion sites after synaptic vesicle fusion and APD release. It should be noted that the absolute values reported here must be evaluated cautiously, while the increases, in general, fit well with the findings in primary cultures.

APDs Inhibit Synaptic Vesicle Exocytosis

To analyze the functional consequences of APD application on synaptic vesicle recycling, we used rat hippocampal neurons

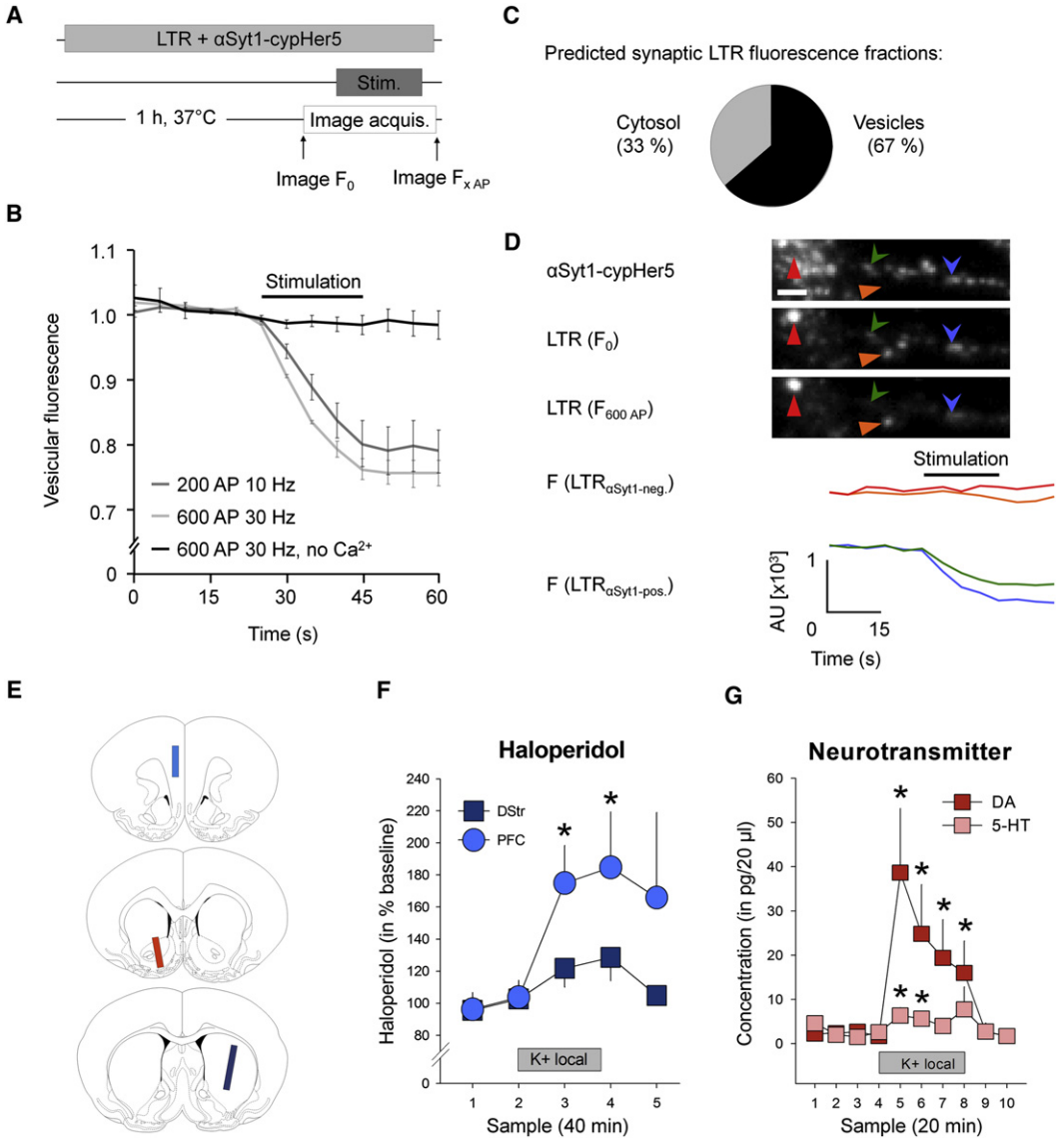

Figure 3. APDs Are Secreted from Presynaptic Terminals during Activity

(A) Scheme of the experimental procedure. The LTR fluorescence intensity was determined before, during, and after the electrical stimulation of LTR- and αSyt1-cypHer5-stained hippocampal neurons.

(B) Normalized LTR fluorescence intensity at synaptic sites over time. Electrical stimulation was performed in the presence (200 AP, 10 Hz and 600 AP, 30 Hz) or absence (0 mM Ca^{2+}, 600 AP, 30 Hz) of calcium ions. LTR is released by electrical stimulation in a calcium-dependent manner.

(C) Pie plot of the LTR fluorescence fractions at synaptic sites. A 20% or 25% dye loss would correspond to the release of 30% or 37% of the vesicular fluorescence, respectively.

(D) Representative images of LTR-stained organelles that colocalize (arrowheads) or do not colocalize (triangles) with synaptic sites, as defined by αSyt1-cypHer5 before (F_0) and after (F_{600AP}) electrical stimulation. Synaptic (αSyt1-positive) and nonsynaptic (αSyt1-negative) LTR fluorescence intensities are indicated over time. LTR is released from αSyt1-cypHer5-positive sites.

(E) In vivo microdialysis experiments in freely moving rats that were chronically treated with HAL (0.5 mg/kg/d) by osmotic minipumps were performed in various brain regions: light blue indicates prefrontal cortex (PFC), red shows nucleus accumbens (Nac), and dark blue represents dorsal striatum (DStr).

(F) Extracellular HAL concentration (mean + SEM) after a local 100 mM K^+ challenge administered by reverse dialysis (gray bar) in the PFC and DStr.

(G) Extracellular concentration of DA and 5-HT in the NAc (n = 5 experiments).

Error bars represent the SD. *p < 0.05, t tests versus last baseline sample.

transfected with spH, an established reporter of exo- and endocytosis (Figure 4A) (Sankaranarayanan et al., 2000). Our experimental setup consisted of 18 electrical stimulations with 50 AP (10 Hz) every 1.5 min. During min 6–18 of the experiment, the cells were perfused with either APDs or vehicle (Figure 4B).

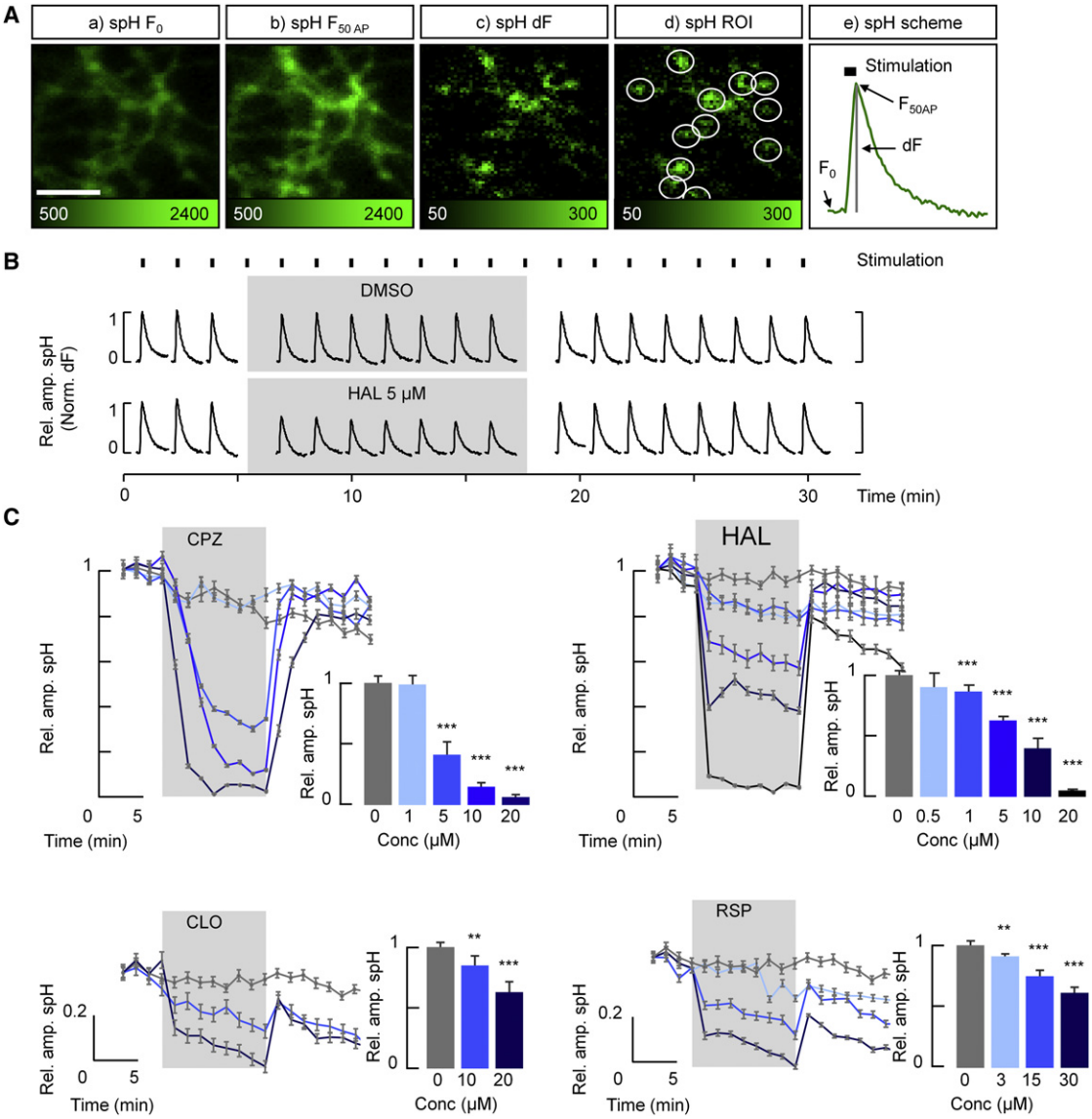

Figure 4. CPZ, HAL, CLO, and RSP Reversibly Reduce Synaptic Vesicle Exocytosis in a Dose-Dependent Manner, as Measured with spH

(A) Image details of rat hippocampal neurons transfected with spH in a representative experiment. The intensity (in arbitrary units) is indicated by color maps. (a) Initial fluorescence intensity (F_0). Scale bar, 5 µm. (b) Fluorescence intensity reached after electrical stimulation with 50 action potentials (AP) at 10 Hz (F_{50AP}). (c) Difference image of (a) and (b) (dF). (d) Automatically detected regions of interest (ROI) marked by white circles. (e) spH time course upon electrical stimulation with a scheme of the calculated parameters. The relative spH amplitudes are normalized to the dF values.

(B) Fluorescence time course in representative experiments. Average fluorescence intensity profiles for the administration of the vehicle (DMSO, 1:1,000, n = 5) and of 5 µM HAL (n = 5). Constant perfusion with standard saline was switched to the vehicle or the drug containing saline during min 6–18. Stimulation, electrical stimulation (50 AP, 10 Hz).

(C) Time courses showing the mean normalized evoked spH fluorescence increase with the maximal concentration-dependent amplitude reduction relative to the vehicle control (column plots) (n = 5 or 6, n > 120). ANOVA: CPZ, $F_{4,103} = 193.92$, $p < 0.001$; HAL, $F_{5,126} = 180.30$, $p < 0.001$; CLO, $F_{2,65} = 20.67$, $p < 0.001$; RSP, $F_{3,80} = 49.81$, $p < 0.001$. Error bars represent SEM. **p < 0.01, ***p < 0.001, t tests.

See Figure S4.

We observed dose-dependent reductions of the evoked exocytosis fluorescence responses upon administration of APDs in contrast to vehicle control (Figure 4C). This reduction was reversible for all four APDs. Compensatory endocytosis of synaptic vesicles was not affected by HAL, CPZ, CLO, and RSP (Figure S4). We conclude that APDs inhibit electrically stimulated synaptic vesicle exocytosis in a dose-dependent manner.

APDs Reduce Presynaptic Calcium Transients

Action potential propagation along the axon results in the influx of Ca^{2+} through voltage-gated ion channels into synaptic

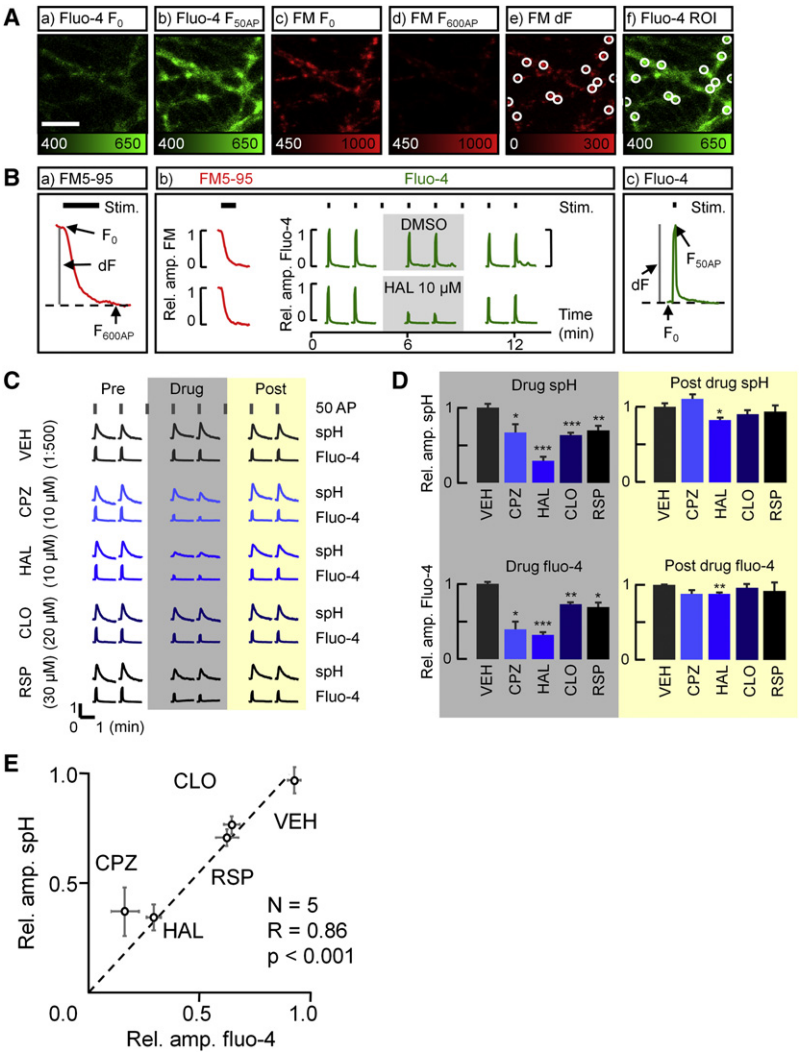

Figure 5. APD-Induced Inhibition of Exocytosis Correlates with a Reduction in Stimulation-Dependent Ca^{2+} Entry

(A) Image details of fluo-4- and FM5-95-stained rat hippocampal neurons in a representative experiment. Scale bar, 5 µm. Intensity scales are indicated for every image. (a) Initial fluorescence intensity of fluo-4-stained cells. Scale bar, 5 µm. (b) Electrical stimulation with 50 action potentials (AP) at 10 Hz provokes a Ca^{2+} influx that leads to an increase in fluo-4 fluorescence. (c) Staining with FM5-95. (d) FM5-95 is unloaded by electrical stimulation with 600 AP at 30 Hz. (e) The difference image between (c) and (d) enables the localization of the synaptic boutons. Automatically detected regions of interest (ROIs) are marked by white circles. (f) The ROIs defined in (e) were used for the fluo-4 analysis.

(B) Average fluorescence intensity profiles for the vehicle (DMSO, 1:1,000) and HAL (10 µM). Synaptic regions were identified by FM5-95 (Ac–Af, Ba, Bb). Subsequent fluo-4 imaging allowed for repetitive measurements of evoked synaptic Ca^{2+} transients (Aa, Ab, Af, Bb, Bc). Constant perfusion with standard saline was switched to either the vehicle or the drug containing saline between min 4.5 and 9. Stim., electrical stimulation (600 AP, 30 Hz for FM5-95 and 50 AP, 10 Hz for fluo-4).

(C) Normalized average fluorescence intensity profiles of spH and fluo-4. Vehicle (VEH, 1:500), CPZ (10 µM), HAL (10 µM), CLO (20 µM), RSP (30 µM). Scale, 1.0 versus 1 min (n = 5, n > 200 for spH; n = 5 or 6, n > 900 for fluo-4).

(D) Mean spH and fluo-4 amplitude reductions relative to the vehicle control during the perfusion of the indicated drug ("Drug") or after the perfusion of the drug ("Post drug"). *p < 0.05, **p < 0.01, ***p < 0.001.

(E) Correlation of the relative fluorescence increase by spH exocytosis and fluo-4-indicated Ca^{2+} influx in the APD and control experiments. The inhibition of Ca^{2+} entry correlates with the inhibition of synaptic vesicle exocytosis (n = 5, R = 0.86; p < 0.001). Values are taken from the experiments depicted in (C). Dotted line shows linear regression (y = ax). p Value is for the hypothesis a = 0. Error bars represent SEM.

boutons, which triggers fast synaptic vesicle exocytosis. Because APDs have been described to have diverse effects on the ion channels involved in this process (Ogata et al., 1989; Sah and Bean, 1994; Wakamori et al., 1989; Yang and Wang, 2005), we next tested whether the observed inhibition of exocytosis is directly linked to ion channel modulation or is the result of effects on the multitude of proteins involved in the assembly and function of the presynaptic vesicle release machinery itself.

We first analyzed the role of calcium channels because Ca^{2+} is directly linked to vesicle release via the Ca^{2+}-sensor synaptotagmin. We measured stimulation-dependent changes in fluo-4-fluorescence while blocking postsynaptic Ca^{2+} influx by AP5 (Koester and Johnston, 2005; Oertner et al., 2002; Schiller et al., 1998). Fluo-4 showed a strong fluorescence increase upon electrical stimulation and Ca^{2+} influx (Figure 5A) (Gee et al., 2000). Synaptic boutons were identified by their activity-dependent FM styryl dye uptake and release (Groemer and Klingauf, 2007), and fluo-4 fluorescence was quantified in these regions (Figure 5A). Similar to the spH experiments (Figure 4), the vehicle control did not alter the presynaptic Ca^{2+} influx evoked by subsequent trains of 50 AP, whereas CPZ, HAL, CLO, and RSP significantly reduced the Ca^{2+} influx (Figures 5B–5D). This inhibition of Ca^{2+} influx was reversible upon drug washout for all of the APDs (Figures 5C and 5D). When comparing the APD-induced amplitude reductions in the evoked fluo-4 and spH fluorescence increases, we found a strong positive correlation (Figure 5E) (R = 0.86; p < 0.001) between the two parameters. Thus, the inhibition of presynaptic Ca^{2+} influx correlated strongly with the inhibition of synaptic vesicle exocytosis for all of the APDs.

Although this result allowed us to conclude that no molecular target within the synaptic vesicle release machinery is involved in the mediation of the APD effect, the reduced Ca^{2+} influx is not sufficient evidence to conclude that calcium channels are a direct target of APDs.

Presynaptic Inhibition of Synaptic Transmission by APDs Is a Result of Sodium Channel Inhibition

Upstream of the Ca^{2+} influx, an APD effect on sodium channels might be responsible for the reduced neurotransmitter release

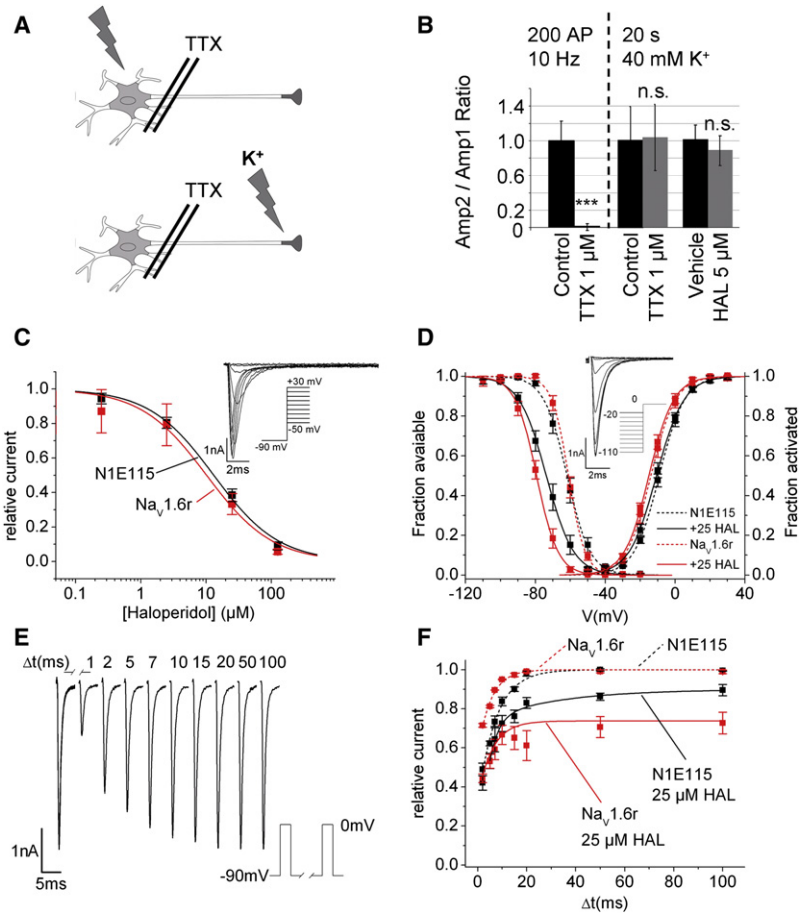

Figure 6. APDs Inhibit Sodium Channels in a State- and Use-Dependent Fashion

(A) Electrical stimulation requires signal propagation along the axon to achieve synaptic transmission and is inhibited by the application of TTX. Chemical stimulation with 40 mM K^+, 20 s (comparable spH amplitude as evoked by 200 AP, 10 Hz) under 1 µM TTX was used to selectively stimulate presynaptic terminals independent of sodium channel action.

(B) Synaptic vesicle exocytosis was reported by spH and monitored before and after drug administration. One micromolar TTX completely blocked vesicular release by electrical stimulation (200 AP 10 Hz). The chemically induced exocytosis was insensitive to TTX and HAL application. ***$p < 0.001$; n.s., not significant; t tests.

(C) Dose-response curves for HAL block of endogenous ($Na_v1.1/Na_v1.2$) and $Na_v1.6r$ current in N1E115 neuroblastoma cells were determined from steady-state recordings using the activation protocol depicted as inset (V_h −90mV).

(D) Steady-state activation curves were constructed from the activation protocol of (A) and the inactivation protocol (depicted as an inset) before and during the application of HAL (25 µM). Data points were fitted with the use of a Boltzmann equation. Half-activation potential V_{mid} was −13.8 ± 1.4mV ($Na_v1.6r$), −13.6 ± 1.0mV ($Na_v1.6r$ plus HAL), −8.9 ± 1.1mV ($Na_v1.1/Na_v1.2$), and −10.7 ± 1.0mV ($Na_v1.1/Na_v1.2$ plus HAL), with $p = 0.004$ for control versus 25 µM HAL in $Na_v1.1/Na_v1.2$. Half-inactivation potential V_{mid} was −61.4 ± 1.1mV ($Na_v1.6r$), −79.3 ± 1.4mV ($Na_v1.6r$ plus HAL), −61.9 ± 1.7mV ($Na_v1.1/Na_v1.2$), and −72.6 ± 2.2mV ($Na_v1.1/Na_v1.2$ plus HAL), with $p = 8.9E-6$ for control versus 25 µM HAL for $Na_v1.6r$ and $p = 1.0E-5$ for control versus 25 µM HAL for $Na_v1.1/Na_v1.2$. There was $p = 0.002$ for a HAL-induced voltage shift of $Na_v1.6r$ versus $Na_v1.1/Na_v1.2$ ($n = 8$ for $Na_v1.6r$, $n = 7$ for $Na_v1.1/Na_v1.2$).

(E) A gradual recovery from inactivation in a double-pulse protocol with an increasing interpulse interval (inset) is shown here for the endogenous current under the control conditions. The test pulse duration was 5 ms. The intervals between test pulses (Δt) are denoted above the peak of the second current response.

(F) Plot summarizing the effect of HAL (25 µM) on the recovery from inactivation. The peak current elicited by the second pulse was normalized to the peak current of the first pulse. The data points were fitted using a biexponential function and were plotted against the interpulse interval. Here, $n = 3$ for $Na_v1.6r$ and $n = 3$ for $Na_v1.1/Na_v1.2$, at 20 ms. Additionally, $p = 0.029$ for control versus 25 µM HAL for $Na_v1.1/Na_v1.2$, and $p = 0.04$ for control versus 25 µM HAL for $Na_v1.6r$.

via exocytosis. This would fit well with previous reports about their modulation by APDs (Ogata et al., 1989).

Thus, we first designed optical experiments to analyze the contribution of sodium channel inhibition by the APDs on vesicle exocytosis. Hippocampal neurons were stimulated either electrically with 200 AP, 10 Hz, or chemically with 40 mM K^+, 20 s, and 1 µM TTX (Figure 6A), which can evoke exocytosis by directly depolarizing the presynaptic terminals in an action potential-independent manner. Both of the stimulation paradigms led to a marked increase in spH fluorescence with comparable amplitudes. An application of the sodium channel blocker TTX (1 µM) almost completely diminished the signal that was evoked by electrical stimulation (Figure 6B). If sodium channels were involved in the inhibition of vesicular exocytosis by APDs, then the exocytosis signal from a high potassium application should not be depressed by APDs. Indeed, the spH amplitude in response to a high potassium application was not significantly reduced upon application of 5 µM HAL (Figure 6B), which points to voltage-gated sodium channels as the primary presynaptic target for APD action.

State- and Use-Dependent Inhibition of Sodium Channels by HAL

We next performed experiments with N1E115 neuroblastoma cells, which generate an endogenous sodium current mediated by TTX-sensitive $Na_v1.1$ and $Na_v1.2$ sodium channels. We transfected the N1E115 cells with a TTX-resistant $Na_v1.6$ mutant and recorded sodium currents during the application of HAL (0.25–125 µM). By adding TTX to the bathing solution, we could distinguish the effects of HAL on the endogenous current mediated by $Na_v1.1$ and $Na_v1.2$ from current solely carried by $Na_v1.6$.

Axons in the central nervous system have been shown to express all three voltage-dependent sodium channel isoforms studied here, with a clear preponderance of $Na_v1.2$ and $Na_v1.6$ (Lorincz and Nusser, 2008). Because the activation threshold of $Na_v1.6$ is considerably lower than that of $Na_v1.2$,

$Na_v1.6$ was assigned the role of axonal "detonator," triggering impulse generation and conduction (Hu et al., 2009; Royeck et al., 2008).

In the first set of experiments, we determined dose-response relationships for the inhibitory action of HAL on the endogenous sodium current and $Na_v1.6$ using a standard activation protocol (Figure 6C, inset). From the dose-response curves depicted in Figure 6C, we calculated that half-maximal inhibition (IC_{50}) of the peak sodium current occurred at 13.1 ± 2.1 μM and 10.2 ± 4.0 μM for $Na_v1.1$/$Na_v1.2$ and $Na_v1.6$, respectively. We then examined the effect of 25 μM HAL on their steady-state activation and inactivation. HAL produced a small but significant leftward shift of the activation curve of the endogenous sodium current, whereas $Na_v1.6$ activation remained unaffected. In contrast, HAL produced a much more pronounced shift of steady-state inactivation to more negative potentials for both endogenous current and $Na_v1.6$ (Figure 6D). The leftward shift of inactivation strongly suggested a preferential binding of HAL to inactivated sodium channels. We calculated (see Supplemental Experimental Procedures) K_i values to be 1.5 μM for $Na_v1.1$/$Na_v1.2$ and 0.18 μM for $Na_V1.6$. These findings indicate that HAL shows a pronounced state-dependent binding, with its affinity to the inactivated state one ($Na_v1.1$/$Na_v1.2$) or even two orders of magnitude ($Na_v1.6$) higher than to the resting state. The preferential binding of HAL to inactivated $Na_v1.6$ is of particular functional significance, given the pivotal role of this Na_v isoform in controlling the axonal excitability.

We next investigated the use dependence of the HAL block by measuring the gradual recovery of the peak sodium current from inactivation in a double-pulse protocol, in which the interpulse interval was increased stepwise (Figure 6E). Under control conditions, endogenous currents and $Na_v1.6$ completely recovered within approximately 20 ms. In the presence of HAL (25 μM), however, both currents exhibited a slower and incomplete recovery (Figure 6F). Together, our data indicate that HAL inhibits high-threshold as well as low-threshold sodium channels of central nervous system axons in a highly state- and use-dependent fashion at concentrations that are well within the therapeutic range.

The Degree of Inhibition of Synaptic Vesicle Exocytosis Is Stimulation Dependent

The use-dependent inhibition of sodium channels should result in a use-dependent inhibition of synaptic vesicle exocytosis. To test this hypothesis, we quantified the inhibition of exocytosis with HAL under weak (60 AP, 40 Hz) and more intense (180 AP, 40Hz) stimulation conditions by monitoring the spH fluorescence response of cultured hippocampal neurons to two identical electrical stimulations 5 min apart. The second stimulus was applied in the presence of the drug or vehicle (Figure 7A). Indeed, increasing the number of APs from 60 to 180 significantly increased the relative inhibition of exocytosis by 5 μM HAL and enabled 0.5 μM HAL to significantly inhibit exocytosis (Figure 7B).

To provide further evidence for an activity-dependent inhibition of exocytosis in the context of preserved neuronal networks, we performed electrophysiological whole-cell recordings from visually identified neurons in hippocampal and NAc slices. Functional consequences of a use-dependent sodium channel inhibition were assessed by applying stimulus trains. Excitatory postsynaptic currents (EPSCs) of hippocampal CA1 pyramidal neurons were measured during a 25 Hz stimulus train of 4 s duration in the absence and presence of two concentrations of HAL (0.5 and 5 μM). Under control conditions, the stimulus train produced an initial increase of the EPSC amplitude, which slowly decayed and approached baseline toward the end of the train (Figures 7C and 7D). The initial rise was also observed in HAL, but EPSCs declined soon below baseline in a dose-dependent fashion (Figures 7C and 7D). The progressive reduction of EPSCs during the train reflects the use dependence of the APD effect and is in line with the fluorescence measurements presented in Figure 7B.

We used two strategies to substantiate our concept that the use-dependent inhibition of EPSC is causally linked to the blockade of voltage-gated sodium channels (Figure 6). First, we demonstrated that the effects of HAL on train-evoked EPSCs could be mimicked by a low concentration of the highly potent and selective sodium channel blocker TTX (25 nM, Figures 7C and 7D). Second, we functionally isolated axonal action potentials and recorded their extracellular equivalent, the so-called fiber volleys (FVs), in the absence and presence of either a low concentration of TTX or several APDs. Under control conditions, FVs exhibited only a small decrement later in the train. In sharp contrast, TTX, which is known to block sodium channels in a use-dependent manner (Conti et al., 1996) as well as all of the three APDs tested (5 μM HAL, 30 μM CPZ, 30 μM RSP), produced a pronounced use-dependent inhibition of FVs (Figure 7E). The depressant effect of APDs on EPSCs during train stimulation is, therefore, sufficiently explained by their inhibitory action on axonal action potentials.

Notably, the effect was not limited to the hippocampus but was also observed in the NAc, which is a major target region of dopaminergic projections and contains mainly medium spiny neurons expressing D1 or D2 DA receptors. The behavior of EPSCs in NAc medium spiny interneurons during stimulus trains was remarkably different from that in hippocampal CA1 pyramidal cells because, even under control conditions, EPSCs displayed only a brief and weak initial enhancement before they progressively decayed (Figures 7F and 7G). As a consequence, the inhibitory effect of HAL (5 μM) was much more pronounced when compared to the hippocampus (Figures 7F and 7G). Importantly, FVs in NAc proved to be approximately equally resistant to stimulus trains compared with hippocampal FVs, and HAL reduced FVs with similar efficacy (Figure 7H). These data indicate that, in the NAc with its dense dopaminergic innervation, transmitter release is especially sensitive to the use-dependent inhibition of axonal sodium channels by APDs.

Effective Inhibition of Exocytosis Requires the Accumulation of APDs in Synaptic Vesicles

To determine whether the accumulation of APDs in synaptic vesicles is required for the efficient inhibition of exocytosis, we assessed the extent of the inhibition induced by 5 μM HAL in the presence of folimycin, which abolished the accumulation of

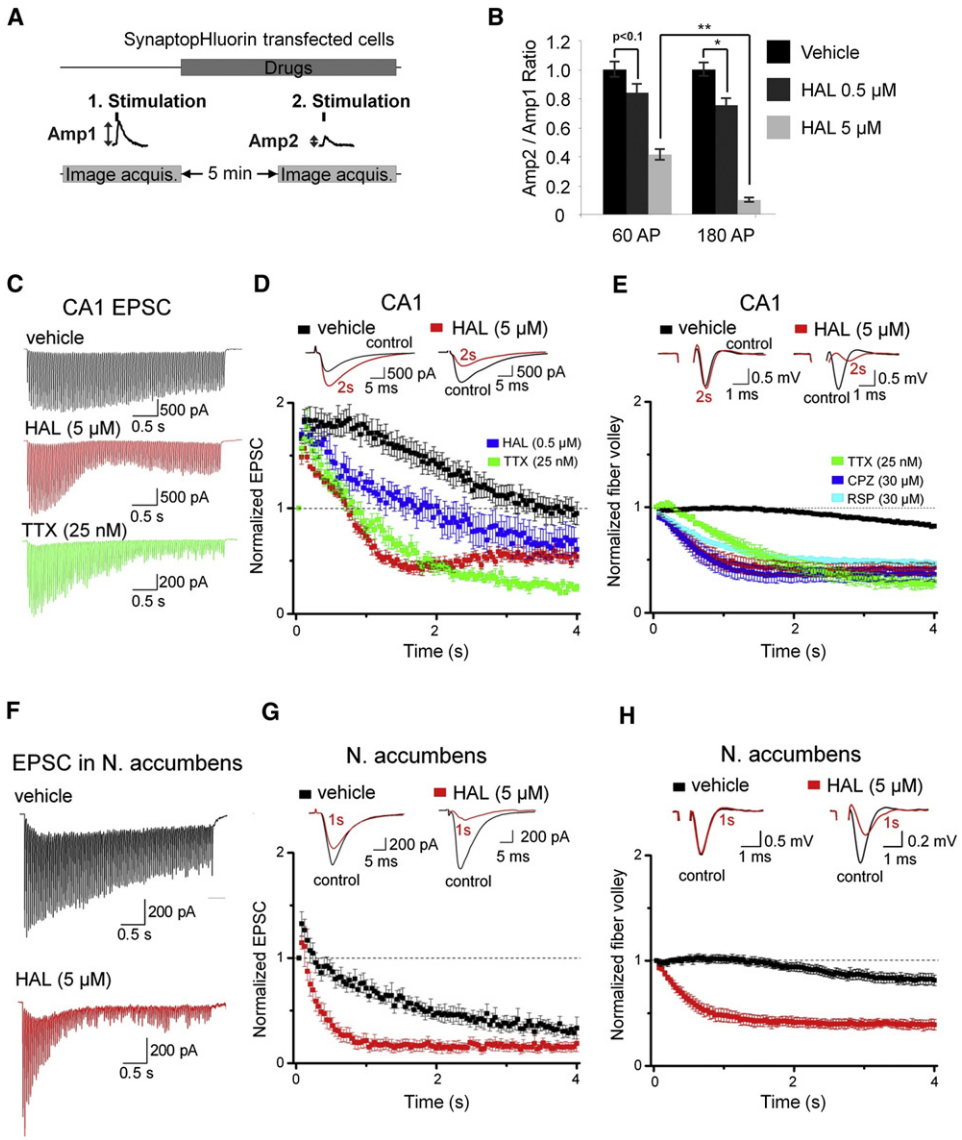

Figure 7. The Inhibition of Synaptic Transmission by APDs Is Use Dependent

(A) Experimental procedure for the optical measurement of use-dependent inhibition. spH-reported electrically induced exocytosis was monitored before and after drug administration.

(B) The ratio of spH fluorescence increases before and after the administration of HAL (0.5 or 5 μM), which was evoked with either 60 or 180 action potentials (AP) at 40 Hz (n = 3 to 6, n > 120). Error bars represent SEM. *p < 0.05, **p < 0.01, n.s. not significant, t tests.

(C and D) The incubation of hippocampal slices with HAL (0.5 and 5 μM) for 2–5 hr dramatically enhanced the use-dependent reduction of EPSC amplitudes (vehicle, n = 5; HAL 0.5 μM, n = 6; HAL 5 μM, n = 5) during 100 stimuli at 25 Hz. This effect was mimicked by low-dose TTX (25 nM, 2–4 hr incubation, n = 5). EPSCs were normalized to their amplitudes before the train. Illustrations in (C) are typical traces from different experiments. Insets depict superimposed EPSCs before and 2 s after the start of a 25 Hz train with and without HAL incubation.

(E) Incubation of hippocampal slices (for 2–5 hr) with HAL (5 μM, n = 7), CPZ (30 μM, n = 5), RSP (30 μM, n = 5), and TTX (25 nM, n = 5) reduced CA1 axonal activity during a 25 Hz train (vehicle n = 11). CA1 FVs were normalized to their amplitudes before the train. Insets depict superimposed FVs before and 2 s after the start of a 25 Hz train.

(F and G) Incubation of slices containing NAc with HAL (5 μM) for 2–6 hr dramatically enhanced the use-dependent inhibition of EPSCs (vehicle, n = 8; HAL 5 μM, n = 7) during 100 stimuli at 25 Hz. Insets depict superimposed EPSCs before and 1 s after the start of a 25 Hz train with and without HAL incubation.

(H) Incubation of NAc slices with HAL (5 μM) for 2–6 hr reduced axonal activity (vehicle, n = 6; HAL 5 μM, n = 6) during 100 stimuli at 25 Hz. Insets depict superimposed FVs before and 1 s after the start of a 25 Hz train.

HAL in synaptic vesicles (Figure 1). Exocytosis was measured with FM4-64 (Figure 8A). The fluorescence of the dye was unaffected by changes of the intravesicular pH value (Figure 2B) or by APD administration (Figure 2D). As expected, 5 μM HAL inhibited the FM4-64 release that occurred in response to stimulation with 600 AP at 30 Hz (Figures 8B and 8C). However, in the presence

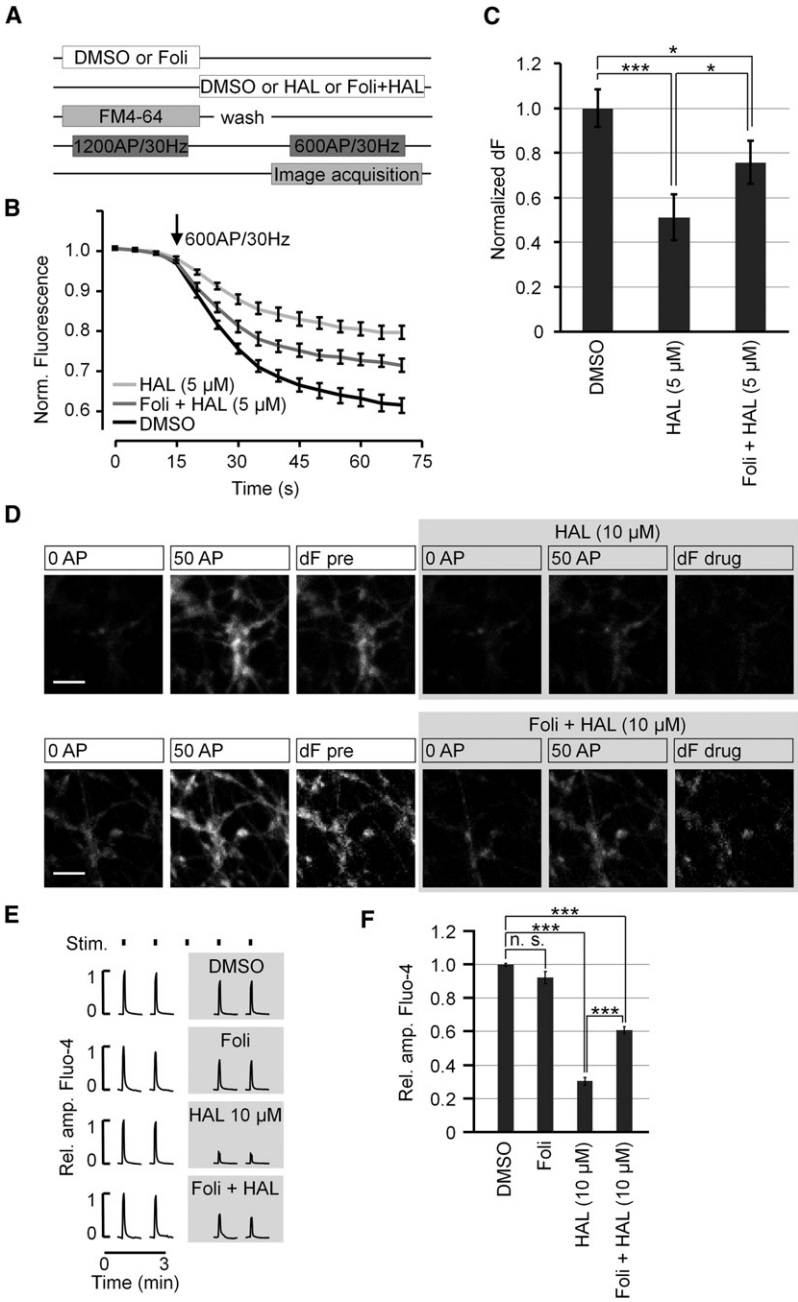

Figure 8. Folimycin Prevents the Efficient Inhibition of Synaptic Vesicle Exocytosis and Calcium Influx by HAL

(A) Experimental procedure for (B) and (C). The destaining of FM4-64-loaded synaptic terminals by 600 AP at 30 Hz was monitored in the presence of either the vehicle (DMSO), HAL (5 µM) or HAL and folimycin (Foli+HAL, 80 nM folimycin and 5 µM HAL).

(B) Normalized fluorescence intensities of FM4-64-stained hippocampal boutons as a function of time.

(C) Normalized ΔF before and after electrical stimulation (n = 4 experiments, n > 150 synapses). Error bars represent SEM. *p < 0.05, ***p < 0.001, t tests.

(D) Image details of fluo-4-stained rat hippocampal neurons from representative experiments. Scale bars, 5 µm. Upper panel illustrates that the ΔF (pre) of fluo4 induced by electrical stimulation with 50 AP at 10 Hz was reduced in the presence of 10 µM HAL (ΔF drug). Lower panel shows that in the presence of 80 nM folimycin, the HAL-induced inhibition of calcium influx was less pronounced.

(E) Normalized average fluorescence intensity profiles of fluo-4 experiments. Vehicle (DMSO, 1:500), folimycin (Foli, 80 nM), HAL (10 µM), and folimycin plus HAL (Foli+HAL, 80 nM folimycin and 10 µM HAL).

(F) Normalized average Δf values of fluo-4 amplitudes relative to the DMSO (n = 2 experiments) control (n = 3–5 experiments, n > 500 synapses). Error bars represent SEM. ***p < 0.001, t tests. n. s., not significant.

See Figure S5.

of folimycin, the inhibition of exocytosis by HAL was significantly ($p < 0.05$) reduced, while the administration of folimycin alone did not affect exocytosis (Figure S5; Sankaranarayanan and Ryan, 2001).

To measure this effect with another pH-independent optical probe, we repeated the experiment with the Ca^{2+}-sensitive dye fluo-4 (Figure 8D). Again, electrical stimulation resulted in a marked increase in fluo-4 fluorescence, which was reduced upon HAL (5 µM) application (Figure 8E). In agreement with the FM experiments described in the previous paragraph, folimycin application significantly decreased the reduction of the fluo-4 amplitude induced by HAL (Figure 8F). Thus, the accumulation of APDs in synaptic vesicles significantly contributes to their inhibitory effects on synaptic vesicle exocytosis.

DISCUSSION

During treatment, APDs and other psychotropic drugs accumulate in the brains of patients. In the present work, we studied the subcellular localization of APD accumulation in acidic organelles and identified functional consequences of this phenomenon. We demonstrated that accumulated APDs are secreted from synaptic vesicles upon exocytosis, leading to increased extracellular drug concentrations during neuronal activity. The secretion of APDs in turn was able to inhibit synaptic transmission in a use-dependent manner.

Increase of Extracellular Concentrations by Activity-Dependent Secretion of APDs

We found that synaptic transmission as measured by synaptic vesicle exocytosis was reduced by APDs in low micromolar concentrations. This concentration range raised our concerns because it has been convincingly demonstrated that the clinical efficacy of APDs correlates with effects observed for nanomolar concentrations (Seeman et al., 1976). Additionally, APDs acutely

inhibit sodium channels in low micromolar concentrations (Figure 6), which in previous work were found unlikely to be achieved extracellularly during APD therapy (Baumann et al., 2004). Thus, instead of therapeutic benefits, continuously present micromolar APD concentrations were related mainly to side effects of the drugs (Ogata et al., 1989).

A major part of our study was, therefore, devoted to demonstrate that the accumulation of APDs in synaptic vesicles (Table 1; Figures 1 and 2) results in high APD concentrations within these confined compartments. Upon activity, synapses release their micromolar APD content into the synaptic cleft (Figure 3). We confirmed the activity-dependent release by in vitro fluorescence microscopy and in vivo data from experiments with freely moving rats treated with HAL. The released APDs have an inhibitory effect on signal propagation by promoting sodium channel inactivation (Figures 6 and 7). Even the extracellular HAL concentrations in the nanomolar range were sufficient to exert a use-dependent inhibitory action under prolonged stimulation (Figures 6 and 7). Accordingly, APD concentrations inhibiting sodium channels are likely to be reached at least locally during neuronal activity. Overall, both inhibition of sodium channels and activity-dependent secretion contribute to the use-dependent action of the drugs. The present work, thus, suggests a mechanism wherein the presence of APDs in synaptic vesicles results in increased extracellular APD concentrations upon neuronal activity, leading to autoinhibitory feedback on synaptic transmission.

Potential Implications of APD Accumulation and Secretion Affecting the Understanding of Therapeutic Actions of APDs

While the therapeutic effect of APDs starts soon after application, it usually reaches its maximum after 4–6 weeks (Agid et al., 2003; Leucht et al., 2005). The effects on synaptic transmission reported here, which are based on the accumulation of the drugs, might contribute to the slow development of the full therapeutic action of the drugs because tissue accumulation occurs within the same time range (Kornhuber et al., 1999). Accordingly, accumulation and secretion effects could explain the beneficial effects of electroconvulsive therapy (ECT) during APD treatment, which are not observed when ECT is performed without APD therapy (Falkai et al., 2005). In light of our findings (Figures 3 and 4), the concentration of APDs available locally is likely to be increased acutely upon ECT-induced seizures.

Physiologically, precisely mediated negative feedback inhibition of neocortical pyramidal cells is necessary for the generation of synchronized high-frequency oscillations, which are related to attention and perception, and whose disturbance has been linked to the pathophysiology of schizophrenia (Uhlhaas and Singer, 2010). Such a deficit in synchronization has, for example, been found in psychotic patients prior to antipsychotic treatment (Gallinat et al., 2004) and chronically ill patients (Ferrarelli et al., 2010; Uhlhaas et al., 2006).

The autoinhibition of synaptic transmission described here by the secretion of accumulated APDs could be beneficial to the generation of synchronized neuronal oscillations in schizophrenia. Our data underline the importance of measuring the neuronal oscillation patterns of unmedicated patients, or patients free of symptoms after sufficient antipsychotic therapy and in an already accumulated drug state. If the secretion of APDs and the associated selective modulation of synaptic transmission were important for the treatment of schizophrenia, then one could further speculate that an enriched environment (Oshima et al., 2003; Tost and Meyer-Lindenberg, 2012) is useful for patients under medication, whereas it would harm the psychotic, not yet treated patient.

Concluding Remarks

Taken together, our study proves the concept of APD accumulation first suggested by Rayport and Sulzer (1995) and defines synaptic vesicles as organelles that exert accumulation- and use-dependent inhibitory functional effects. Although we found more pronounced inhibitory effects of APDs in striatal tissue (Figure 7), which hosts the receptors that bind the drugs in nanomolar concentrations (in this case DA receptors), our current results are limited with respect to other substance classes or synapse types. It will therefore be interesting to investigate the autoinhibitory effects of psychotropic drugs accumulated in synaptic vesicles on specific network activity profiles within cortical (Goto et al., 2010) and subcortical (Kellendonk, 2009) pathways as well as various neurotransmitter systems (Lisman et al., 2008), especially DA signaling, and differential effects of other classes of psychotropic drugs (Sulzer, 2011).

EXPERIMENTAL PROCEDURES

Ethics Statement

All animal work was approved by the Kollegiales Leitungsgremium of the Franz-Penzoldt Zentrum, Erlangen and was conducted in conformity with the Animal Protection Law of the Federal Republic of Germany and the guidelines of the State of Bavaria.

Cell Culture and Transfection

Hippocampal neuronal cultures were prepared from 1- to 4-day-old Wistar rats. Briefly, newborn rats were sacrificed by decapitation. The hippocampus was removed from each brain and was transferred into ice-cold Hank's salt solution, and the dentate gyrus was cut away. After digestion with trypsin (5 mg ml^{-1}), cells were triturated mechanically and plated in MEM, supplemented with 10% fetal calf serum and 2% B27 Supplement (all from Invitrogen, Taufkirchen, Germany). If required, neurons were transfected on DIV3 (days in vitro) with spH (Sankaranarayanan et al., 2000) under the control of a synapsin promoter with a modified calcium phosphate method by Threadgill et al. (1997). Experiments were performed between DIV25 and DIV30.

N1E115 neuroblastoma cells were maintained at 37°C in 5% CO_2 in DMEM (Invitrogen) with 5 g/l glucose and were supplemented with 10% fetal bovine serum (Biochrom, Berlin) and 1% penicillin/streptomycin solution (Biochrom). Cells were trypsinized and plated in 3.5 cm dishes (Corning, Lowell, MA, USA). For recordings from $Na_V1.6r$, N1E115 cells were transfected on the next day with 1 μg of cDNA for each dish and 0.5 μg of pEGFP-C1 (Mountain View, CA, USA) with Nanofectin (PAA, Pasching, Austria) according to the manufacturers' protocol. The $mNa_V1.6$ was a gift from E. Leipold and S. Heinemann (Leipold et al., 2006). The TTX-resistant variant mNaV1.6r Y371S was constructed with the use of the QuikChange II XL Site-Directed Mutagenesis Kit (Agilent Technologies, Santa Clara, CA, USA).

Imaging

Experiments were conducted at room temperature on a Nikon TI-Eclipse inverted microscope (60×, 1.2 NA water-immersion objective; Perfect Focus System). Fluorescence was excited by a Nikon Intensilight C-HGFI through excitation filters centered at 482, 561, and 628 nm using dichroic long-pass

mirrors (cutoff wavelength 500, 570, and 660 nm, respectively). The emitted light passed emission band-pass filters ranging from 500 to 550 nm, 570 to 640 nm, and 660 to 730 nm (Semrock, Rochester, NY, USA) and was projected onto a cooled EM-CCD camera (iXonEM DU-885 or iXonEM DU-897; Andor).

Coverslips were placed into a perfusion chamber. Please see the Supplemental Experimental Procedures for a description of solutions, dyes, antibodies, and inhibitors for the individual experiments. Throughout the experiments, perfusion was kept constantly at 0.2 ml/min (Fast-Step Valve Control Perfusion System VC-77SP8; Warner Instruments). Fast solution exchanges were achieved by a piezo-controlled stepper device (SF-77B; Warner Instruments) using a three-barrel glass tubing. Synaptic boutons were stimulated by electric field stimulation (platinum electrodes, 10 mm spacing, 1 ms pulses of 50 mA and alternating polarity).

Recorded image stacks were used to automatically detect spots of synaptic bouton size (Sbalzarini and Koumoutsakos, 2005), where an electrically evoked fluorescence increase (spH and fluo-4) or decrease (FM dyes) occurred in difference images. For LTR DND-99 (Invitrogen, Karlsruhe) experiments, synapses labeled with an anti-Synaptotagmin1 antibody were detected by a Laplace-operator-based peak detection method by Dorostkar et al. (2010). All image and data analysis was performed using custom-written routines in MATLAB (The MathWorks, Natick, MA, USA). SpH and fluo-4 fluorescence was normalized to the mean stimulation-dependent difference in fluorescence (ΔF) before drug application.

Photoconversion and Electron Microscopy

Rat hippocampal neurons were incubated with 500 nM LTR for 1 hr at 37°C and subsequently fixed in 2.5% glutaraldehyde in PBS. Illumination for the photoconversion of LTR was performed through a 20× 0.5 NA objective (Olympus, Hamburg, Germany) with green light (550 nm) for 45–60 min in the presence of a 1.5 mg/ml DAB solution. Photoconversion of FM1-43 and further electron microscope processing followed a standard protocol by Denker et al. (2009).

Electrophysiology

Transverse slices containing hippocampus and coronal slices containing NAc (350 μm thick) were prepared from 1-month-old rats. Electrophysiological signals were filtered at 1 kHz and sampled at 10 kHz using a MultiClamp 700B amplifier in conjunction with a Digidata 1440A interface and pClamp10 software (all from Molecular Devices, Sunnyvale, CA, USA). Whole-cell recordings of visualized CA1 pyramidal cells and NAc medium spiny neurons were performed in artificial cerebrospinal fluid (aCSF, see Supplemental Experimental Procedures). Patch pipettes were filled with 135 mM K-gluconate, 5 mM HEPES, 3 mM $MgCl_2$, 5 mM EGTA, 2 mM Na_2ATP, 0.3 mM NaGTP, and 4 mM NaCl (pH 7.3). Constant current pulses (pulse width 0.1 ms, 60–400 μA) were delivered to a concentric bipolar tungsten-stimulating electrode positioned in CA1 stratum radiatum and in NAc to evoke synaptic currents in pyramidal cells and NAc neurons, respectively. Glutamatergic EPSCs were recorded at −80mV (after correcting liquid junction potentials) and were pharmacologically isolated by perfusing slices with picrotoxin (100 μM), APV (50 μM), and CGP 55845 (2 μM). Field potentials arising from axonal action potentials (FVs) were evoked by a bipolar electrode (pulse width 0.1 ms) and were recorded in CA1 stratum radiatum or NAc with extracellular recording pipettes filled with modified aCSF (in which bicarbonate was replaced with HEPES to avoid a pH change). Synaptic responses were abrogated by a combination of low-calcium aCSF (0.5 mM $CaCl_2$, 3.5 mM $MgCl_2$), picrotoxin, and the ionotropic glutamate receptor antagonist kynurenic acid (2 mM).

In neuroblastoma N1E115 cells transfected with a TTX-resistant $Na_v1.6$, sodium currents carried by the TTX-resistant $Na_v1.6r$ mutant were isolated by adding 1 μM TTX (Biotrend, Wangen/Zurich, Switzerland) to the bath. Current signals were recorded in whole-cell voltage-clamp mode at room temperature (21°C ± 1°C). Recordings were sampled at 20 kHz (low-pass filter 5 kHz) using an Axopatch 200A amplifier in conjunction with a Digidata 1322A interface and pClamp10 software. For details on the measurement protocols and the solutions used, please refer to the Supplemental Experimental Procedures.

Microdialysis

Guide cannulae (MAB6.14, Microbiotech) were implanted into male Sprague-Dawley rats targeting the medial PFC, caudate-putamen, and NAc, as described in Pum et al. (2008). After 5–6 days of recovery, osmotic minipumps (Samaha et al., 2007) were implanted and used to deliver HAL (0.5 mg/kg/d; i.p.) over a period of 14 days. During the experiments a 100 mM K^+ challenge was applied for 80 min by reverse dialysis, before the perfusion medium was changed back to aCSF. HAL analysis was performed by LC-MS/MS with online extraction. DA and 5-HT analysis was performed by high-performance liquid chromatography with electrochemical detection (Pum et al., 2008).

Cell Model of APD Accumulation

The accumulation of APDs in synaptic vesicles was assessed using a mathematical model based on the Fick-Nernst-Planck equation (Trapp et al., 2008) (Zhang et al., 2010), as described in detail in the Supplemental Experimental Procedures. Properties of the test compounds given in Table 1 were estimated using ACD (ACD/LogD Suite version 10.04, 2007; Advanced Chemistry Development, Toronto), and therapeutic plasma levels for CPZ, HAL, CLO, and RSP were taken from Baumann et al. (2004).

Statistical Analysis

Statistical analysis was performed using MATLAB. Error bars indicate SEM unless otherwise indicated. To analyze the effects of treatment, ANOVA was used. For single-group comparisons, unpaired t tests were applied. These tests were performed using built-in routines in MATLAB.

SUPPLEMENTAL INFORMATION

Supplemental Information includes five figures and Supplemental Experimental Procedures and can be found with this article online at doi:10.1016/j.neuron.2012.04.019.

ACKNOWLEDGMENTS

We would like to thank Drs. Erwin Neher and Peter Uhlhaas for critically reading this manuscript and Katrin Ebert for expert technical assistance. This work was supported by the Erlanger Leistungsbezogene Anschubfinanzierung und Nachwuchsförderung ELAN Grant Nr. PS-08.09.22.2 and by the Interdisciplinary Center of Clinical Research (IZKF) in Erlangen (Project J5) (both to T.W.G.). E.M.W. was supported by a stipend from the Erlanger Leistungsbezogene Anschubfinanzierung und Nachwuchsförderung ELAN. The funders had no role in the study design, the data collection and analysis, the decision to publish, or the preparation of the manuscript.

Accepted: April 3, 2012
Published: June 6, 2012

REFERENCES

Adie, E.J., Kalinka, S., Smith, L., Francis, M.J., Marenghi, A., Cooper, M.E., Briggs, M., Michael, N.P., Milligan, G., and Game, S. (2002). A pH-sensitive fluor, CypHer 5, used to monitor agonist-induced G protein-coupled receptor internalization in live cells. Biotechniques *33*, 1152–1154, 1156–1157.

Agid, O., Kapur, S., Arenovich, T., and Zipursky, R.B. (2003). Delayed-onset hypothesis of antipsychotic action: a hypothesis tested and rejected. Arch. Gen. Psychiatry *60*, 1228–1235.

Amato, D., Natesan, S., Yavich, L., Kapur, S., and Müller, C.P. (2011). Dynamic regulation of dopamine and serotonin responses to salient stimuli during chronic haloperidol treatment. Int. J. Neuropsychopharmacol. *14*, 1327–1339.

Baumann, P., Hiemke, C., Ulrich, S., Eckermann, G., Gaertner, I., Gerlach, M., Kuss, H.J., Laux, G., Müller-Oerlinghausen, B., Rao, M.L., et al; Arbeitsgemeinschaft fur neuropsychopharmakologie und pharmakopsychiatrie. (2004). The AGNP-TDM expert group consensus guidelines: therapeutic drug monitoring in psychiatry. Pharmacopsychiatry *37*, 243–265.

Chen, H.T., and Kandasamy, S.B. (1996). Effect of chloral hydrate on in vivo KCl-induced striatal dopamine release in the rat. Neurochem. Res. *21*, 695–700.

Conti, F., Gheri, A., Pusch, M., and Moran, O. (1996). Use dependence of tetrodotoxin block of sodium channels: a revival of the trapped-ion mechanism. Biophys. J. *71*, 1295–1312.

de Duve, C., de Barsy, T., Poole, B., Trouet, A., Tulkens, P., and Van Hoof, F. (1974). Commentary. Lysosomotropic agents. Biochem. Pharmacol. *23*, 2495–2531.

Denker, A., Kröhnert, K., and Rizzoli, S.O. (2009). Revisiting synaptic vesicle pool localization in the *Drosophila* neuromuscular junction. J. Physiol. *587*, 2919–2926.

Dorostkar, M.M., Dreosti, E., Odermatt, B., and Lagnado, L. (2010). Computational processing of optical measurements of neuronal and synaptic activity in networks. J. Neurosci. Methods *188*, 141–150.

Duvvuri, M., Gong, Y., Chatterji, D., and Krise, J.P. (2004). Weak base permeability characteristics influence the intracellular sequestration site in the multidrug-resistant human leukemic cell line HL-60. J. Biol. Chem. *279*, 32367–32372.

Falkai, P., Wobrock, T., Lieberman, J., Glenthoj, B., Gattaz, W.F., and Möller, H.J. (2005). World Federation of Societies of Biological Psychiatry (WFSBP) guidelines for biological treatment of schizophrenia, part 1: acute treatment of schizophrenia. World J. Biol. Psychiatry *6*, 132–191.

Ferrarelli, F., Peterson, M.J., Sarasso, S., Riedner, B.A., Murphy, M.J., Benca, R.M., Bria, P., Kalin, N.H., and Tononi, G. (2010). Thalamic dysfunction in schizophrenia suggested by whole-night deficits in slow and fast spindles. Am. J. Psychiatry *167*, 1339–1348.

Freedman, R. (2003). Schizophrenia. N. Engl. J. Med. *349*, 1738–1749.

Gallinat, J., Winterer, G., Herrmann, C.S., and Senkowski, D. (2004). Reduced oscillatory gamma-band responses in unmedicated schizophrenic patients indicate impaired frontal network processing. Clin. Neurophysiol. *115*, 1863–1874.

Gee, K.R., Brown, K.A., Chen, W.N., Bishop-Stewart, J., Gray, D., and Johnson, I. (2000). Chemical and physiological characterization of fluo-4 Ca(2+)-indicator dyes. Cell Calcium *27*, 97–106.

Gemperle, A.Y., Enz, A., Pozza, M.F., Lüthi, A., and Olpe, H.R. (2003). Effects of clozapine, haloperidol and iloperidone on neurotransmission and synaptic plasticity in prefrontal cortex and their accumulation in brain tissue: an in vitro study. Neuroscience *117*, 681–695.

Goto, Y., Yang, C.R., and Otani, S. (2010). Functional and dysfunctional synaptic plasticity in prefrontal cortex: roles in psychiatric disorders. Biol. Psychiatry *67*, 199–207.

Groemer, T.W., and Klingauf, J. (2007). Synaptic vesicles recycling spontaneously and during activity belong to the same vesicle pool. Nat. Neurosci. *10*, 145–147.

Harrison, P.J., and Weinberger, D.R. (2005). Schizophrenia genes, gene expression, and neuropathology: on the matter of their convergence. Mol. Psychiatry *10*, 40–68.

Hu, W., Tian, C., Li, T., Yang, M., Hou, H., and Shu, Y. (2009). Distinct contributions of Na(v)1.6 and Na(v)1.2 in action potential initiation and backpropagation. Nat. Neurosci. *12*, 996–1002.

Kapur, S. (2003). Psychosis as a state of aberrant salience: a framework linking biology, phenomenology, and pharmacology in schizophrenia. Am. J. Psychiatry *160*, 13–23.

Kapur, S., VanderSpek, S.C., Brownlee, B.A., and Nobrega, J.N. (2003). Antipsychotic dosing in preclinical models is often unrepresentative of the clinical condition: a suggested solution based on in vivo occupancy. J. Pharmacol. Exp. Ther. *305*, 625–631.

Kellendonk, C. (2009). Modeling excess striatal D2 receptors in mice. Prog. Brain Res. *179*, 59–65.

Koester, H.J., and Johnston, D. (2005). Target cell-dependent normalization of transmitter release at neocortical synapses. Science *308*, 863–866.

Kornhuber, J., Schultz, A., Wiltfang, J., Meineke, I., Gleiter, C.H., Zöchling, R., Boissl, K.W., Leblhuber, F., and Riederer, P. (1999). Persistence of haloperidol in human brain tissue. Am. J. Psychiatry *156*, 885–890.

Kornhuber, J., Weigmann, H., Röhrich, J., Wiltfang, J., Bleich, S., Meineke, I., Zöchling, R., Härtter, S., Riederer, P., and Hiemke, C. (2006). Region specific distribution of levomepromazine in the human brain. J. Neural Transm. *113*, 387–397.

Kornhuber, J., Henkel, A.W., Groemer, T.W., Städtler, S., Welzel, O., Tripal, P., Rotter, A., Bleich, S., and Trapp, S. (2010). Lipophilic cationic drugs increase the permeability of lysosomal membranes in a cell culture system. J. Cell. Physiol. *224*, 152–164.

Korpi, E.R., Kleinman, J.E., Costakos, D.T., Linnoila, M., and Wyatt, R.J. (1984). Reduced haloperidol in the post-mortem brains of haloperidol-treated patients. Psychiatry Res. *11*, 259–269.

Leipold, E., Hansel, A., Borges, A., and Heinemann, S.H. (2006). Subtype specificity of scorpion beta-toxin Tz1 interaction with voltage-gated sodium channels is determined by the pore loop of domain 3. Mol. Pharmacol. *70*, 340–347.

Leucht, S., Busch, R., Hamann, J., Kissling, W., and Kane, J.M. (2005). Early-onset hypothesis of antipsychotic drug action: a hypothesis tested, confirmed and extended. Biol. Psychiatry *57*, 1543–1549.

Lisman, J.E., Coyle, J.T., Green, R.W., Javitt, D.C., Benes, F.M., Heckers, S., and Grace, A.A. (2008). Circuit-based framework for understanding neurotransmitter and risk gene interactions in schizophrenia. Trends Neurosci. *31*, 234–242.

Lorincz, A., and Nusser, Z. (2008). Cell-type-dependent molecular composition of the axon initial segment. J. Neurosci. *28*, 14329–14340.

Miesenböck, G., De Angelis, D.A., and Rothman, J.E. (1998). Visualizing secretion and synaptic transmission with pH-sensitive green fluorescent proteins. Nature *394*, 192–195.

Oertner, T.G., Sabatini, B.L., Nimchinsky, E.A., and Svoboda, K. (2002). Facilitation at single synapses probed with optical quantal analysis. Nat. Neurosci. *5*, 657–664.

Ogata, N., Yoshii, M., and Narahashi, T. (1989). Psychotropic drugs block voltage-gated ion channels in neuroblastoma cells. Brain Res. *476*, 140–144.

Oshima, I., Mino, Y., and Inomata, Y. (2003). Institutionalisation and schizophrenia in Japan: social environments and negative symptoms: nationwide survey of in-patients. Br. J. Psychiatry *183*, 50–56.

Pum, M.E., Huston, J.P., De Souza Silva, M.A., and Müller, C.P. (2008). Visual sensory-motor gating by serotonin activation in the medial prefrontal and occipital, but not in the rhinal, cortices in rats. Neuroscience *153*, 361–372.

Rayport, S., and Sulzer, D. (1995). Visualization of antipsychotic drug binding to living mesolimbic neurons reveals D2 receptor, acidotropic, and lipophilic components. J. Neurochem. *65*, 691–703.

Royeck, M., Horstmann, M.T., Remy, S., Reitze, M., Yaari, Y., and Beck, H. (2008). Role of axonal NaV1.6 sodium channels in action potential initiation of CA1 pyramidal neurons. J. Neurophysiol. *100*, 2361–2380.

Sah, D.W., and Bean, B.P. (1994). Inhibition of P-type and N-type calcium channels by dopamine receptor antagonists. Mol. Pharmacol. *45*, 84–92.

Samaha, A.N., Seeman, P., Stewart, J., Rajabi, H., and Kapur, S. (2007). "Breakthrough" dopamine supersensitivity during ongoing antipsychotic treatment leads to treatment failure over time. J. Neurosci. *27*, 2979–2986.

Sankaranarayanan, S., and Ryan, T.A. (2001). Calcium accelerates endocytosis of vSNAREs at hippocampal synapses. Nat. Neurosci. *4*, 129–136.

Sankaranarayanan, S., De Angelis, D., Rothman, J.E., and Ryan, T.A. (2000). The use of pHluorins for optical measurements of presynaptic activity. Biophys. J. *79*, 2199–2208.

Sbalzarini, I.F., and Koumoutsakos, P. (2005). Feature point tracking and trajectory analysis for video imaging in cell biology. J. Struct. Biol. *151*, 182–195.

Schikorski, T., and Stevens, C.F. (1997). Quantitative ultrastructural analysis of hippocampal excitatory synapses. J. Neurosci. *17*, 5858–5867.

Schiller, J., Schiller, Y., and Clapham, D.E. (1998). NMDA receptors amplify calcium influx into dendritic spines during associative pre- and postsynaptic activation. Nat. Neurosci. *1*, 114–118.

Schmalzing, G. (1988). The role of a transmembrane pH gradient in uptake and release of imipramine and haloperidol in synaptosomes. Mol. Pharmacol. *34*, 888–895.

Seeman, P., Lee, T., Chau-Wong, M., and Wong, K. (1976). Antipsychotic drug doses and neuroleptic/dopamine receptors. Nature *261*, 717–719.

Strange, P.G. (2001). Antipsychotic drugs: importance of dopamine receptors for mechanisms of therapeutic actions and side effects. Pharmacol. Rev. *53*, 119–133.

Sulzer, D. (2011). How addictive drugs disrupt presynaptic dopamine neurotransmission. Neuron *69*, 628–649.

Threadgill, R., Bobb, K., and Ghosh, A. (1997). Regulation of dendritic growth and remodeling by Rho, Rac, and Cdc42. Neuron *19*, 625–634.

Tost, H., and Meyer-Lindenberg, A. (2012). Puzzling over schizophrenia: schizophrenia, social environment and the brain. Nat. Med. *18*, 211–213.

Trapp, S., Rosania, G.R., Horobin, R.W., and Kornhuber, J. (2008). Quantitative modeling of selective lysosomal targeting for drug design. Eur. Biophys. J. *37*, 1317–1328.

Tsuneizumi, T., Babb, S.M., and Cohen, B.M. (1992). Drug distribution between blood and brain as a determinant of antipsychotic drug effects. Biol. Psychiatry *32*, 817–824.

Uhlhaas, P.J., and Singer, W. (2010). Abnormal neural oscillations and synchrony in schizophrenia. Nat. Rev. Neurosci. *11*, 100–113.

Uhlhaas, P.J., Linden, D.E., Singer, W., Haenschel, C., Lindner, M., Maurer, K., and Rodriguez, E. (2006). Dysfunctional long-range coordination of neural activity during Gestalt perception in schizophrenia. J. Neurosci. *26*, 8168–8175.

Wakamori, M., Kaneda, M., Oyama, Y., and Akaike, N. (1989). Effects of chlordiazepoxide, chlorpromazine, diazepam, diphenylhydantoin, flunitrazepam and haloperidol on the voltage-dependent sodium current of isolated mammalian brain neurons. Brain Res. *494*, 374–378.

Welzel, O., Henkel, A.W., Stroebel, A.M., Jung, J., Tischbirek, C.H., Ebert, K., Kornhuber, J., Rizzoli, S.O., and Groemer, T.W. (2011). Systematic heterogeneity of fractional vesicle pool sizes and release rates of hippocampal synapses. Biophys. J. *100*, 593–601.

Yang, T.T., and Wang, S.J. (2005). Effects of haloperidol and clozapine on glutamate release from nerve terminals isolated from rat prefrontal cortex. Synapse *56*, 12–20.

Zhang, X., Zheng, N., Zou, P., Zhu, H., Hinestroza, J.P., and Rosania, G.R. (2010). Cells on pores: a simulation-driven analysis of transcellular small molecule transport. Mol. Pharm. *7*, 456–467.